Astronomy & Astrophysics manuscript no. paper February 3, 2015
(DOI: will be inserted by hand later)

A pilot study of the radio-emitting AGN population: the emerging new class of FR 0 radio-galaxies

Ranieri D. Baldi[1,2,3], Alessandro Capetti[4], and Gabriele Giovannini[5,6]

[1] SISSA-ISAS, via Bonomea 265, I-34136 Trieste, Italy
[2] Physics Department, The Technion, 32000, Haifa, Israel; e-mail: baldi@ph.technion.ac.il
[3] Physics Department, Faculty of Natural Sciences, University of Haifa, 31905, Haifa, Israel
[4] INAF - Osservatorio Astrofisico di Torino, Strada Osservatorio 20, I-10025 Pino Torinese, Italy
[5] Dipartimento di Fisica e Astronomia, Università di Bologna, via Ranzani 1, 40127 Bologna, Italy
[6] INAF-Istituto di Radio Astronomia, via P. Gobetti 101, I-40129 Bologna, Italy

Abstract. We present the results of a pilot JVLA project aimed at studying the bulk of the radio-emitting AGN population, unveiled by the NVSS/FIRST and SDSS surveys. The key questions are related to the origin of their radio-emission and to its connection with the properties of their hosts.

We obtained A-array observations at the JVLA at 1.4, 4.5, and 7.5 GHz for 12 sources, a small but representative sub-sample. The radio maps reveal compact unresolved or slightly resolved radio structures on a scale of 1-3 kpc, with only one exception of a hybrid FR I/FR II source extended over ∼40 kpc. Thanks to the new high-resolution maps or to the radio spectra, we isolate the radio core component in most of them.

The sample splits into two groups. Four sources have small black hole (BH) masses (mostly $\sim 10^7$ $M_\odot$) and are hosted by blue galaxies, often showing evidence of a contamination from star formation to their radio emission and associated with radio-quiet (RQ) AGN. The second group consists in seven radio-loud (RL) AGN, which live in red massive ($\sim 10^{11}$ $M_\odot$) early-type galaxies, with large BH masses ($\gtrsim 10^8$ $M_\odot$), and spectroscopically classified as Low Excitation Galaxies (LEG), all characteristics typical of FR I radio galaxies. They also lie on the correlation between radio core power and [O III] line luminosity defined by FR Is. However, they are more core dominated (by a factor of ∼30) than FR Is and show a deficit of extended radio emission. We dub these sources 'FR 0' to emphasize their lack of prominent extended radio emission, the single distinguishing feature with respect to FR Is.

The differences in radio properties between FR 0s and FR Is might be ascribed to an evolutionary effect, with the FR 0 sources undergoing to rapid intermittency that prevents the growth of large scale structures. However, this contrasts with the scenario in which low luminosity radio-galaxies are fed by continuous accretion of gas from their hot coronae. In our preferred scenario the lack of extended radio emission in FR 0 is due to their smaller jet Lorentz Γ factor with respect to FR Is. The slower jets in FR 0s are more subject to instabilities and entrainment, causing their premature disruption.

Key words. galaxies: active – galaxies: elliptical and lenticular, cD – galaxies: nuclei - galaxies: jets – radio continuum: galaxies

1. Introduction

The advent of large area surveys with high sensitivity and the cross-match of radio and optical data opened the possibility to use large samples of extragalactic sources to investigate the links between the radio properties, the central engine, and the host galaxies. Based on the recent results of Baldi & Capetti (2009) and Baldi & Capetti (2010), a new population of radio-emitting sources turns out to dominate in the local Universe.

Best et al. (2005) built a sample of 2215 radio-galaxies (RGs) by cross-correlating the SDSS (DR2), NVSS, and FIRST datasets (hereafter the SDSS/NVSS sample). This sample is selected at $F_{1.4} > 5$ mJy and it includes RGs up to $z \sim 0.3$, covering the range of radio luminosity $L_{1.4} \sim 10^{22} - 10^{26}$ W Hz^{-1}. All morphologies are represented, including twin-jets and core-jet FR Is, narrow and wide angle tails, and FR IIs. However, most of them (∼ 80 %) are unresolved or barely resolved at the 5″ FIRST resolution.

The SDSS/NVSS sample is mostly (∼90%) composed of RL AGN, representing the bulk of the RGs population (with a space density > 100 times higher than 3C sources) but it is virtually unexplored. A few partial results have been already obtained, even though the radio data available are extremely limited, generally only FIRST and NVSS images with angular resolution problems and the missing radio spectral coverage (they are generally too faint to be detected in the existing high frequency surveys). In a previous paper Baldi & Capetti (2010) found the following results on this sample:

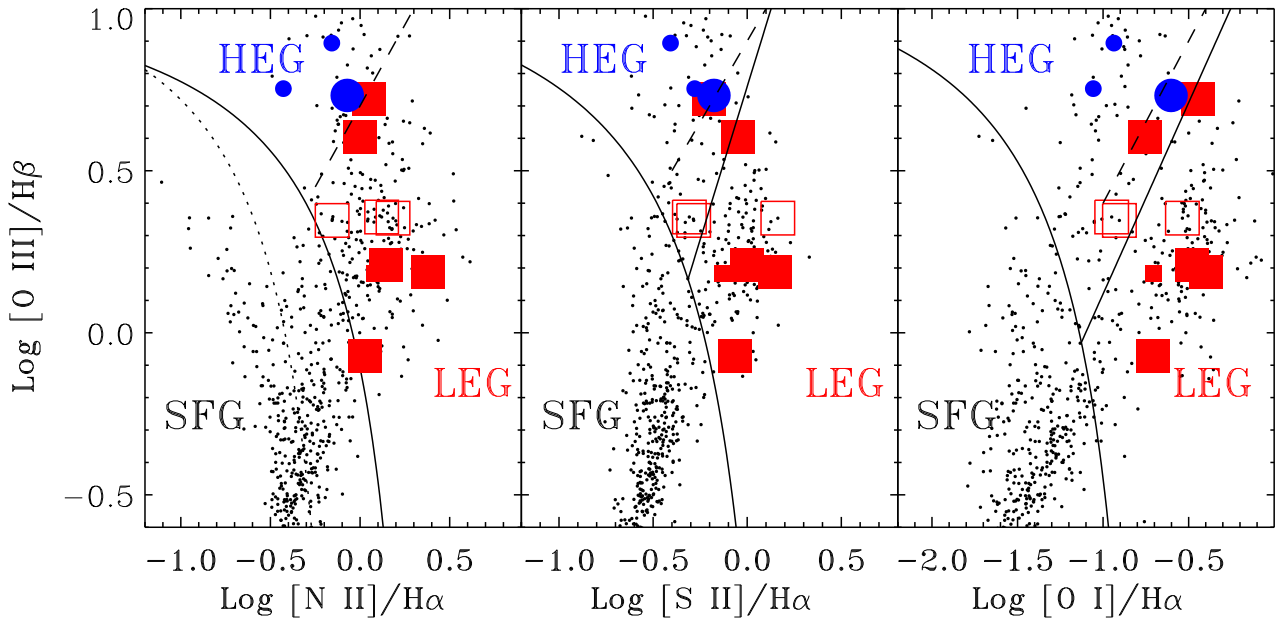

Fig. 1. Spectroscopic diagnostic diagrams for the galaxies of the sample. The small dot points correspond to the SDSS/NVSS sample studied by Baldi & Capetti (2010), while the symbols in color represent galaxies with the new JVLA observations. The solid lines are from Kewley et al. (2006) and separate star-forming galaxies (SFG), LINER, and Seyfert. In the first panel the region between the two curves is populated by the composite galaxies. The dashed lines instead separate RL AGN into HEG from LEG (Buttiglione et al. 2010) which roughly correspond to Seyfert and LINER classification for RL AGN. The red squares are the LEGs, while the blue circles are the HEGs. The large filled symbols are associated with BH masses $>10^8$ $M_\odot$, large empty with $\sim 10^{7.7}$ $M_\odot$, and small symbols with $<10^{7.3}$ $M_\odot$.

1) the AGN power estimated from the optical line luminosity of the SDSS/NVSS sample is at the same level of classical FR I RGs. However, the sample shows a deficit of a factor ~100 of radio emission with respect to the 3C sources with the same optical power.

2) the SDSS/NVSS sample generally shows optical emission line ratios typical of AGN: most of them (~ 70%) can be classified as Low Excitation Galaxies (LEG) similarly to the FR Is, but a substantial fraction of High Excitation Galaxies (HEG) is also present[1].

3) Most of the hosts of the SDSS/NVSS are statistically indistinguishable from those of 3C sources from the point of view of morphology, color, stellar and black hole masses. They are generally associated with giant elliptical galaxies, with no signs of star formation, located in dense environment. Thus the deficit in radio emission cannot be ascribed to differences in their hosts.

4) A small fraction (~10%) of the sample shows rather different photometric properties and it represents the RQ AGN contamination to the main population of RL AGN.

These results have been recently confirmed by the analysis of a larger sample, obtained from the SDSS DR7, by Best & Heckman (2012).

Similar results to the analysis of the SDSS/NVSS sample come from a parallel study of a sample of 14 nearby giant early-type galaxies (ETGs) of extremely low radio luminosity (10^{20-22} W Hz^{-1} at 1.4 GHz) (Baldi & Capetti 2009). They are named CoreG and are much fainter than FR Is (Balmaverde & Capetti 2006). Despite the low radio power, the CoreG host genuine "miniature" RL nuclei, indistinguishable from the FR Is. In fact they extend the FR I relations at different wavelengths (Chiaberge et al. 1999; Balmaverde et al. 2006; Balmaverde & Capetti 2006; Baldi et al. 2010), indicat-

[1] We bear in mind that HEG galaxies in the 3C catalog are all FR II RGs (Buttiglione et al. 2010)

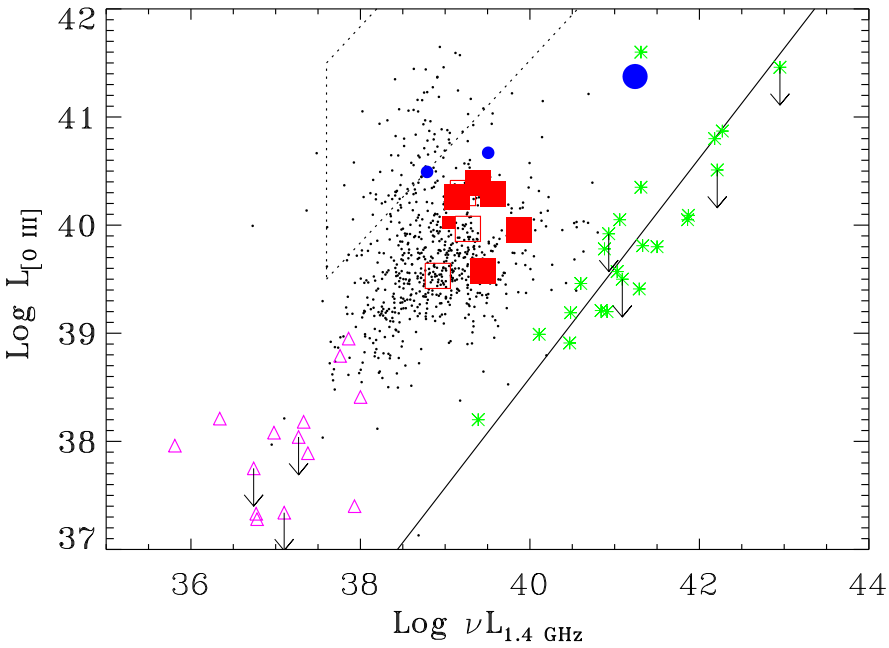

Fig. 2. FIRST vs [O III] line luminosity (erg s^{-1}). The colored points represent the 12 galaxies observed with the JVLA coded as in Fig. 1. The small dot points correspond to the SDSS/NVSS sample studied by Baldi & Capetti (2010) . The solid line represents the correlation between line and radio-luminosity derived for the 3CR/FR I sample. The dotted lines include the region where Seyfert galaxies are found. The empty pink triangles are the CoreG and the green stars are the 3CR/FRIs.

ing a common synchrotron origin of the nuclear emission. However, CoreG show a less extended radio structure and a core dominance up to ∼100 times higher than FR Is, but similar to the SDSS/NVSS sample. A high core dominance is generally interpreted as evidence of Doppler boosting in a radio source oriented at a small angle with respect to the line of sight. The correlation found with the core radio power and emission line luminosity (independent of orientation) indicates that we are seeing a genuine deficit of extended radio emission and that no geometric effect is present.

However, the differences between CoreG and FR Is might be driven by their much lower radio luminosity. For this reason a high resolution radio study of the SDSS/NVSS sample, objects sharing the same range of power of FR Is, is required. In fact, the radio properties of the bulk of the RL population are virtually unexplored and we have little or no information on their radio morphology or on their spectral properties. This severely hampers our ability to understand their nature and how they are related, on the one hand, to classical RGs and, on the other hand, to low luminosity AGN. An improvement of the radio data is needed to provide us with a more complete view of the radio emission phenomenon.

We then undertook a project aimed at understanding the nature of the radio emission of such objects and its connection with the host galaxies. Precisely, we present new high-resolution observations with the JVLA of a pilot sample of 12 sources selected from the SDSS/NVSS sample. We obtained A array observations in L and C bands, reaching a resolution of 0.″2. In particular, the C band provides us with the possibility of measuring the high frequency core emission, crucial for our purposes.

We aim at answering the following questions:

1) which is the nature of the radio emission: star formation, radio outflows as in RQ AGN or genuine emission from a relativistic jet as in RL AGN?

2) once we isolate the RL AGN, which is their level of core dominance? Are they highly core dominated similarly to the CoreG, but unlike the 3C sources? Or, alternatively, they are just compact, but with well developed extended radio structures which produce most of the radio emission?

3) do they follow the relation between radio core and line emission defined by 3C/FR Is? The new observations aim at isolating their genuine radio core emission, an essential information to test their nuclear similarity with the FR Is.

4) is their radio structure characterized by jet(s), diffuse plumes or a double-lobed morphology? Are these jets one or two sided? The distribution of jet sidedness will constrain their speed.

5) which is the fraction of Compact Steep Spectrum in the sample?

6) is there a relationship between the radio properties and the optical spectroscopic classification, i.e., HEG and LEG differ from the point of view of their radio structure?

The paper is organized as follows. In Sect. 2 we define the sample. Section 3 presents the new JVLA observations for 12 sources. In Sect. 4 we analyze the radio and spectro-photometric properties of the sample. We discuss the results in Sect. 5, presenting a new class of radio-sources, FR 0s

(Sect. 5.1). The summary and conclusions to our findings are given in Sect. 6. We provide the notes on the radio properties of the sources which show extended morphology in the Appendix A.

2. The sample

The objects observed with the JVLA have been extracted from the SDSS/NVSS Best et al. sample adopting the following criteria:

- redshift $z < 0.1$,
- the main optical emission lines detected at least 5 σ significance (for the Hβ we relaxed this requirement to 3 σ) to ensure a reliable spectral classification,
- equivalent width for the [O III] lines larger than 3 Å and with a measurement error smaller than 1 Å; this ensures that the line emission is associated with an AGN and not with a stellar origin (Capetti & Baldi 2011),
- declination in the range $-10 < \delta < 10$ in order to optimize the observing strategy.

This procedure returns 68 objects. Twelve of them have been then randomly selected for the observations. In Tab. 1 we give the main properties of the observed objects.

We use the spectroscopic diagnostic diagrams defined by Buttiglione et al. (2010) for the 3CR sample to recognize the nature of their nuclear emission. These diagnostics are formed by pairs of nuclear emission line ratios, to separate active nuclei from star-forming galaxies (e.g. Baldwin et al. 1981), and, furthermore to differentiate AGN into branches of different excitation level, i.e. low-excitation galaxies (LEG) and high-excitation galaxies (HEG). This separation is similar to that introduced by Kewley et al. (2006) as diagnostic to separate among the RQ AGN population, LINER and Seyfert (Heckman 1980).

From the point of view of their optical spectral classification, our sample covers the whole range of ionization (Fig. 1), with eight objects located into the LEG area and two objects falling into in the HEG region. Two objects (ID 590 and 625) straddle the separation between the two classes; we classify 590 (625) as LEG (HEG) since in 2 out of three diagnostic ratios it is consistent with such a classification.

In Fig. 2 we show their location in a diagram comparing the FIRST radio and optical [O III]. All objects show a large deficit of radio emission when compared to the FR Is part of the 3C sample by a factor ranging from $\sim$ 30 to $\sim$ 1000. They are all (but one) located in the region of higher density of the SDSS/NVSS sample, just avoiding the lowest line luminosity, due to the third requirement for their selection. ID 656 is on the boundary of the region of RQ Seyferts. Only one object (ID 625) falls in a poorly populated area, being one of the objects of higher radio and line luminosity. In Fig. 2 we also stress the similarity of our sample to the CoreG sample in terms of $L_{FIRST}/L_{[O\,III]}$ ratio.

Fig. 3 shows the SDSS optical images of the galaxies of the sample. Most of the targets has an optical morphology akin of elliptical galaxies. Some, namely ID 519, 537, 547 and 568, show edge-on disks, while 567 shows spiral arms.

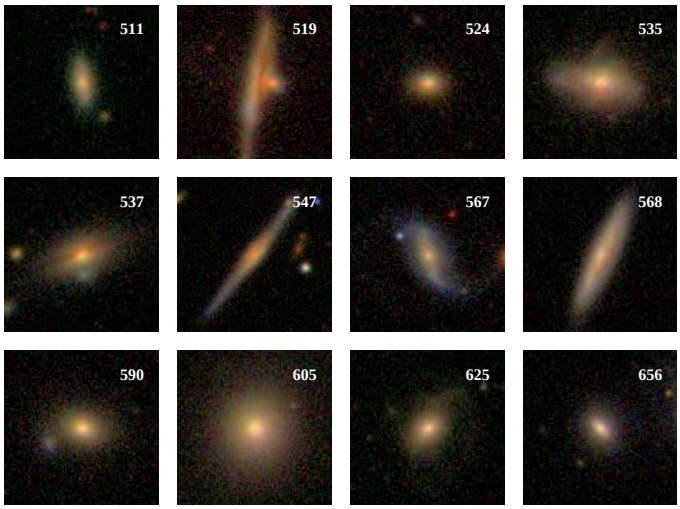

Fig. 3. SDSS optical images of the galaxies of our sample. The size of each frame is $40'' \times 40''$.

Table 1. The sample

ID	R.A.	Dec.	z	F_{NVSS}	F_{FIRST}	$F_{[O\ IIII]}$
511	353.1122	-1.2017	0.094	3.2	1.57	92
519	354.0168	0.0798	0.076	18.6	16.53	138
524	356.5379	0.9858	0.093	24.8	25.92	43
535	359.4337	-0.1749	0.076	7.2	4.70	133
537	0.4175	1.0920	0.061	6.5	6.49	38
547	5.1446	-0.4708	0.072	10.7	9.53	75
567	9.9076	-0.3288	0.055	<8.3	2.86	148
568	8.6813	-0.0408	0.042	57.0	56.01	1161
590	15.2546	-0.4123	0.097	7.3	5.13	106
605	18.8158	0.2135	0.045	42.4	46.52	81
625	27.0677	0.3292	0.092	600.2	519.95	114
656	43.3733	-0.2349	0.029	<23.7	6.96	1676

Column description: (1) name; (2)-(3) coordinates of the optical source; (4) redshift; (5)- (6) radio flux at 1.4 GHz from NVSS and FIRST surveys (mJy); (7) [O III] emission line flux (10^{-17} erg s^{-1} cm^{-2}).

3. The JVLA observations

We obtained 6 hours of observations with the JVLA of NRAO[2] with A array configuration in 3 days on December 2012 and January 2013. We observed 12 objects in scans of 2 hours for each group composed of 4 sources. Each source was observed for ~20 minutes spaced out by the pointing to the phase calibrators (J0022+0014, J0059+0006,J0217+0144, and J2337-0230). The flux calibrator was 3C 48 observed for ~6-7 minutes. The observations were performed in L and C bands; the exposure time was split in the two band configurations. While the L band configuration corresponds to the default 1GHz-wide band centered at 1.4 GHz, the C band was modified based on our purpose. We divide the available 2-GHz bandwidth into two sub-band of 1 GHz centered at 4.5 and 7.5 GHz. This strategy allows to obtain images in 3 different radio frequencies in two

[2] The National Radio Astronomy Observatory is a facility of the National Science Foundation operated under cooperative agreement by Associated Universities, Inc.

Table 2. Results of the JVLA observations

ID	Morph.	F_{tot}	F_{core}	beam	rms
511	SR	1.15		1.″2	0.04
	1″	0.34	0.29	0.″4	0.015
	1.8 kpc	0.26	0.26	0.″2	0.01
519	SR	12.21	9.4	1.″2	0.05
	0.″9	3.8	2.92	0.″4	0.04
	1.3 kpc	2.2	1.96	0.″2	0.013
524	SR	25.42		1.″2	0.04
	0.″3	13.21		0.″4	0.05
	0.5 kpc	9.16		0.″2	0.05
535	P	4.91		1.″2	0.05
		2.24		0.″4	0.02
	<0.3 kpc	1.86		0.″2	0.015
537	P	5.00		2.″2 x 1.″2	0.07
		3.57		0.″4	0.1
	<0.2 kpc	2.99	2.99	0.″2	0.02
547	twosid. jet	12.22		1.″7 x 1.″0	0.05
	2″	4.30		0.″7 x 0.″5	0.02
	2.8 kpc	2.62	0.93	0.″2	0.01
567	P	3.30		2.″0 x 1.″0	0.04
		0.85		0.″4	0.02
	<0.2 kpc	0.74		0.″2	0.01
568	double	37.9		2.″6 x 2.″1	0.04
	1″	27		0.″4	0.06
	0.8 kpc	13.2		0.″35	0.02
590	elongated	5.9		1.″5 x 1.″1	0.03
	0.″8	3.5		0.″4	0.03
	1.5 kpc	2.5		0.″25	0.02
605	P	44.3		2.″1 x 1.″3	0.02
		42.1		0.″6 x 0.″5	0.02
	<0.9 kpc	36.5		0.″25	0.04
625	hybrid	420		1.″1 x 0.″9	0.03
	22″	144	32.3	0.″6 x 0.″4	0.03
	37 kpc	103	31.5	0.″24 x 0.″21	0.02
656	SR	7.4		1.″8 x 1.″6	0.06
	0.″8	–	–	–	–
	0.5 kpc	–	–	–	–

Column description: (1) name; (2) radio morphology (P stands for point-source and SR for slightly resolved), size of the source in arcoseconds and in kpc in the three following rows, (3) total radio flux (mJy) respectively at 1.4 GHz, 4.5 GHz and 7.5 GHz in the three following rows; (4) radio core flux (mJy) respectively at 1.4 GHz, 4.5 GHz and 7.5 GHz in the three following rows; (5) beam size (arcseconds) at 1.4 GHz, 4.5 GHz and 7.5 GHz in the three following rows; (6) rms (mJy) at 1.4 GHz, 4.5 GHz and 7.5 GHz in the three following rows.

integration scan. Each of the three bands was configured in 7 sub-bands of 64 channels of 1 MHz. The object ID 656 has been observed only in L-band due to a telescope failure.

The data reduction was performed with *AIPS* (Astronomical Image Processing System) package according to standard procedures. The final image was then produced from the calibrated data set by *CLEAN*ing to convergence. The final map was obtained using the task *IMAGR* with a beam size ranging between ∼0.″2 and ∼2.″6, according to the band, and different weights to increase the signal to noise ratio. We self-calibrated the maps of the sources with the gain flux $\gtrsim$10 mJy. The core component parameters have been measured with the task *JMFIT*.

The noise level was measured in background regions near the target. The final noise is strongly affected (mainly in L band) by the presence of interferences within the large bandwidth. At high frequency some observations show a gain error in a few telescopes that we were not able to recover in the calibration phase. Since in some sources the total flux density is too low to properly self-calibrate the data in gain (∼10 mJy or less) and even in phase (a few mJy or less), all these problems produced final images with a measured noise level higher than the expected thermal noise.

In Tab. 2 we collect the radio properties. In particular we give the total and core (when visible in the radio images) flux densities in the 3 observing bands.

Table 3. Radio flux ratio

ID	F_{FIRST}/F_{NVSS}	$F_{1.4\ GHz}/F_{NVSS}$	$F_{1.4\ GHz}/F_{FIRST}$	R
511	0.49	0.36	0.73	0.08
519	0.89	0.66	0.74	0.11
524	1.05	1.02	0.98	<0.37
535	0.65	0.68	1.04	0.26
537	1.00	0.77	0.77	0.46
547	0.89	1.14	1.28	0.09
567	–[a]	–[a]	1.15	0.26[b]
568	0.98	0.66	0.71	<0.23
590	0.70	0.81	1.15	0.34
605	1.10	1.04	0.95	0.86
625	0.87	0.70	0.81	0.05
656	–[a]	–[a]	1.06	–

Column description: (1) name; (2) flux ratio between FIRST and NVSS; (3) ratio between 1.4-GHz flux from JVLA observation and NVSS flux; (4) ratio between 1.4-GHz flux from JVLA observation and FIRST flux; (5) core dominance R, i.e. ratio between 7.5-GHz core flux and NVSS flux. [a] two point-like FIRST sources are blended into a single NVSS catalog entry and [b] the core dominance is estimated from the FIRST flux.

4. Results

4.1. Radio properties

The FIRST radio maps of the selected objects show unresolved compact radio sources on a scale of 5″, with the exception of ID 625 which is extended on a scale of ∼ 35″.

In the JVLA observations, most of the sources appears unresolved or slightly resolved down to a resolution of ∼0.″2 which corresponds to 0.2–0.4 kpc. Some sources show instead radio structures on a scale of 1-3 kpc: ID 547 (a twin-jet source), ID 568 (a double source and lacking of the radio core), and ID 590 (with an elongated radio morphology on a scale of 0.″8, possibly due to a bent two-sided jet structure). Finally, ID 625 shows a hybrid radio-structure (Gopal-Krishna & Wiita 2000), being a FR I on the North side and a FR II on the South side on a scale of ∼40 kpc. Tab. 2 collects all the radio properties derived from the new observations. Appendix A provides additional comments on the radio maps for the sources which show extended structures (Figures from A.1 to A.4).

One of the main purposes of our program is to isolate the radio core component and to measure the core dominance of the sources of our sample. However, the high resolution JVLA observations required with this aim and obtained with relatively short exposure time might be missing faint extended emission. In order to explore this possibility we compared the JVLA 1.4 GHz fluxes with those measured by FIRST and NVSS (see Table 3). The JVLA/FIRST flux ratios range from 0.71 to 1.28, with an average value of 0.95 indicating that we recovered most of the radio emission. The comparison with the NVSS data is more complex due to the low resolution of this survey. Indeed, in two cases (namely ID 567 and ID 656) two point-like FIRST sources are blended into a single NVSS catalog entry. Leaving these two sources aside, the JVLA/NVSS flux ratios cover a range between 0.36 and 1.14, with an average of 0.78. We conclude that our measurement recover most of the total radio flux of our sources. In general, the fraction of missing flux is sufficiently small and it does not to alter our view of the overall radio structure.

We obtained matched-beam radio maps to derive the radio spectra at the three frequencies (see Fig. 4). For the object ID 656 it is not possible to derive its spectrum because of the lack of its C-band observation.

In Fig. 4 we report the spectral slope α ($F_\nu \propto \nu^\alpha$), obtained between 1.4 and 4.5 GHz. The spectral indices range from -1.16 to -0.04, indicative of both steep and flat spectra. We note that source 568 shows a strong steepening at 7.5 GHz. This might be due to some missing flux at the highest frequency, although we note that its double structures at 4.5 and 7.5 GHz are very similar. We suggest that the radio lobes spectra might be intrinsically steep.

One of the key point of this study is the measurement of the radio core. The high resolution radio maps at 7.5-GHz reveals a radio core component for five sources (ID 511, 519, 537, 547, and 625). For the remaining sources, we can use the radio spectra to measure the core emission. Two sources (ID 590 and 605) show an overall flat ($\alpha > -0.5$) radio spectrum, consistent with a self-absorbed synchrotron emission; the flux at 7.5 GHz is dominated by the radio core emission. For ID 535 and 567 a spectral flattening occurs at 7.5 GHz where the core emerges over the optically-thin radio emission. For the last three objects of the sample we use the total flux at 7.5 GHz as upper limit for the radio core measurement.

Having measured the radio core component thanks to the new observations, we can include our sources in the L_{core} vs. $L_{[O\,III]}$ plane (Fig. 5), similarly to what done for CoreG in Baldi & Capetti (2009). The radio core power distribution span a range similar to the local 3CR/FR Is. Several sources lie in the same region of the 3CR/FR Is also considering their line luminosities, but others show a radio core deficit (or line excess) with respect to the relation defined by the FR Is. The sources classified as LEGs, on average, lie closer to the relation than the HEGs.

The core dominance of our sources, R, is defined as the ratio between the source nuclear emission at 7.5 GHz and the total flux density, for which we adopt the NVSS measurement (Table 3). We preferred to use the 7.5 GHz core measurements, with respect to the usual definition based on 5 GHz data, to limit as much as possible the contamination from the extended structures. The core dominance ranges between 0.05 and 0.86. The smallest R belongs to the most extended object, the FR I/FR II ID 625.

4.2. Spectro-photometric properties

We now explore the physical properties of the present objects based on the optical spectroscopic and photometric information available from the SDSS survey. We consider the mass of their central black hole (BH), the host mass and morphology, and the $D_n(4000)$ index (see Tab. 4), similarly to the study of SDSS/NVSS sample by Baldi & Capetti (2010).

We estimate the BH mass ($M_{\rm BH}$) from the stellar velocity dispersion adopting the relation of Tremaine et al. (2002). They range from $\sim 10^7$ to $\sim 10^9$ $M_\odot$. The sources are associated with galaxies with a distribution of masses[3] in the range 10^{10}–$10^{11.5}$ $M_\odot$ (and a median of $\sim 10^{11}$ $M_\odot$).

We then study the host type by using the concentration index C_r (defined as the ratio of the radii including 90% and 50% of the light in the r band respectively). ETGs have $C_r \geq 2.86$ (e.g. Strateva et al. 2001; Kauffmann et al. 2003; Bell et al. 2003). This cut basically corresponds to E type with a small contamination of S0 and Sa (Bernardi et al. 2010). A less conservative selection of ETGs uses $C_r \geq 2.60$ (e.g. Nakamura et al. 2003; Shen et al. 2003), which yields a larger contribution from S0 and Sa.

The 4000Å break strength, $D_n(4000)$ (defined as the ratio between the fluxes in the wavelength range 3850-3950Å and 4000–4100Å) is instead sensitive to the presence of a young stellar population (Balogh et al. 1999). Massive galaxies (log $M_*/M_\odot \gtrsim 10.5$) shows a bimodal distribution of $D_n(4000)$ (Kauffmann et al. 2003). The transition between the two groups is located approximately at $D_n(4000) \sim 1.7$ with the red (blue) hosts having larger (smaller) values.

A further diagnostic panel tool enables us to to qualitatively measure the amount of contamination in radio emission in the galaxy due to star formation. This method is based on the location of a galaxy in the $D_n(4000)$ versus $L_{1.4\ \rm GHz}/M_*$ plane, where M_* is the galaxy's stellar mass. Best et al. (2005) predict the radio emission per unit of galaxy mass expected from a stellar population of a given age: when a galaxy shows an excess larger than 0.225 in $D_n(4000)$ above the curve corresponding to the prediction of a star formation event lasting 3 Gyr and exponentially decaying, its radio emission is associated with the AGN.

Figure 6, in the left panel, shows the distribution of the objects in the spectro-photometric diagram composed of C_r vs. $D_n(4000)$, while in the right panel we compare $L_{1.4\ \rm GHz}/M_*$ and $D_n(4000)$. In order to explore the properties of the sample, we separated the sources into three groups based on the BH masses: large $>10^8$ $M_\odot$, intermediate $\sim 10^{7.7}$ $M_\odot$ and small $<10^{7.3}$ $M_\odot$.

[3] M_* is estimated from the g and z SDSS magnitudes following following Bell et al. (2007) resulting in slightly different masses from those reported by Best et al. (2005).

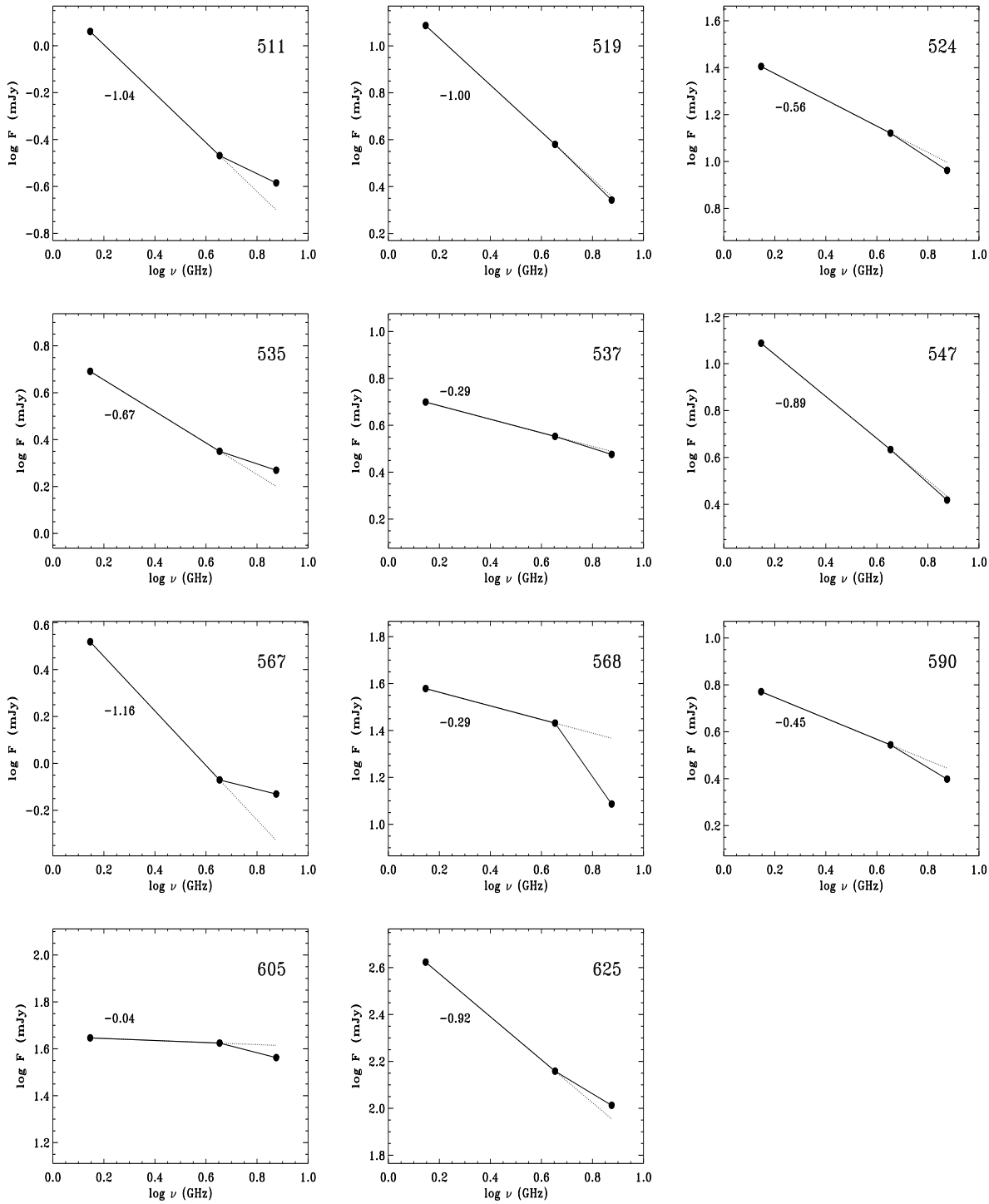

Fig. 4. Radio spectra of the 11 objects observed with JVLA observed at 1.4, 4.5 and 7.5 GHz. The dotted line is the extrapolation of the 1.4-4.5 GHz slope which is reported in each panel.

We note a different behavior of the sources in our sample, related with their BH mass. A first group consists in 4 sources with small (and one intermediate) BH masses, namely ID 511, 567, 568, and 656. Three of them (see Fig. 6, right panel), have a likely contribution of a star formation to their radio emission; this is supported also by their large NVSS/FIRST radio flux ratios, an indication of the presence extended diffuse radio emission, missed by the FIRST images. The fourth object (ID 568) is consistent with being a Seyfert 2 galaxy, based on its location in Fig. 2 and on its spectrophotometric properties. They are all blue galaxies, having $D_n(4000) < 1.6$. In the diagram comparing the core power, L_{core}, and emission line luminosity (Fig. 5) they all show a large deficit of radio core emission, typ-

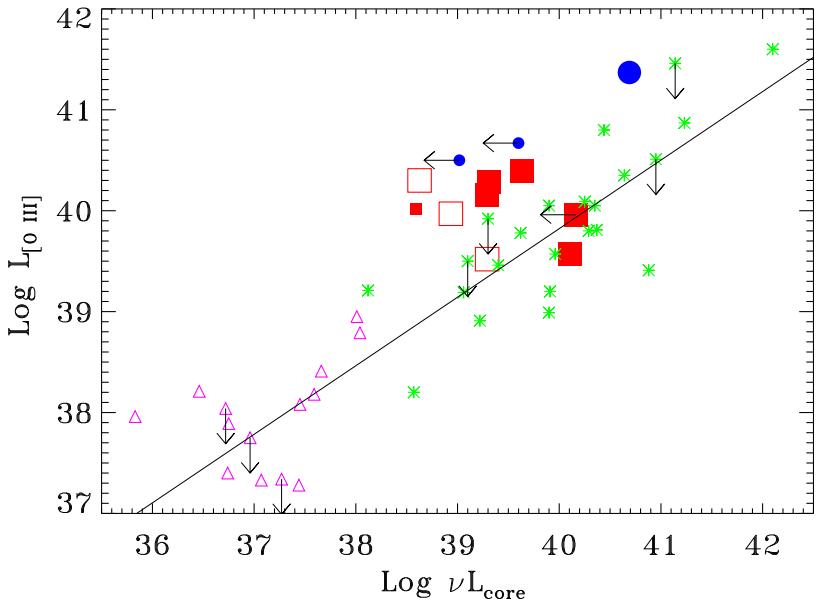

Fig. 5. Core radio power vs. [O III] line luminosity (erg s^{-1}) for CoreG (pink triangles), 3CR/FR I radio-galaxies (green stars), and our sample (colored symbols like in Fig. 1). The line indicates the best linear the for 3CR/FR Is.

Table 4. Spectroscopic and photometric properties

ID	opt. class	$D_n(4000)$	C_r	M_r	Log M_*	Log M_{BH}	Log $L_{[O\ III]}$	Log L_{FIRST}	Log L_{NVSS}	Log L_{core}	radio class
511	LEG	1.52	2.63	-21.74	11.10	7.65	40.30	38.68	38.99	38.63	RQ
519	LEG	1.74	2.42	-22.11	11.30	8.67	40.28	39.50	39.56	39.31	FR 0
524	LEG	1.89	2.87	-21.50	11.07	8.32	39.96	39.89	39.87	<40.16	FR 0
535	LEG	1.75	2.83	-22.61	11.48	8.76	40.26	38.96	39.14	39.29	FR 0
537	LEG	1.95	2.87	-21.38	11.09	7.72	39.52	38.90	38.90	39.29	FR 0
547	LEG	1.67	3.57	-21.62	11.18	7.64	39.97	39.22	39.27	38.93	FR 0
567	LEG	1.44	2.69	-20.95	10.62	7.14	40.02	38.45	<38.91	38.59	RQ
568	HEG	1.56	2.33	-20.99	10.76	7.19	40.67	39.50	39.51	<39.60	RQ
590	LEG	1.93	3.29	-22.47	11.42	8.43	40.39	39.22	39.37	39.64	FR 0
605	LEG	1.99	3.10	-21.86	11.15	8.57	39.57	39.47	39.44	40.10	FR 0
625	HEG	1.61	3.17	-22.13	11.24	8.18	41.37	41.18	41.24	40.69	FR I/FR II
656	HEG	1.39	3.16	-19.25	9.97	7.08	40.50	38.26	<38.79	<39.02	RQ

Column description: (1) name; (2) optical spectroscopic classification; (3) color based on $D_n(4000)$ (typical error 0.07−0.14); (4) concentration index (typical error 0.01−0.03); (5) M_r absolute r-band magnitude (typical error <0.02); (6) galaxy stellar mass M_* ($M_\odot$) (typical error 0.15); (7) black hole mass M_{BH} ($M_\odot$) (typical error 0.07−0.12); (8) [O III] luminosity (erg s^{-1}) (typical error 3−10%); (9) 1.4 GHz FIRST luminosity (erg s^{-1}); (10) 1.4 GHz NVSS luminosity (erg s^{-1}) used as total radio luminosity L_{tot}; (11) 7.5 GHz VLA luminosity (erg s^{-1}) used as radio core luminosity L_{core}; (12) radio class: radio-quiet (RQ) AGN, FR 0, hybrid FR I/FR II.

ically a factor of $\gtrsim$100 , with respect to the relation defined by 3CR/FR Is.

Conversely, the second group includes sources with large/intermediate BH masses, whose radio emission is dominated by the AGN. With the sole exception of ID 625 (the hybrid FR I/FRII radio source) they are associated with red massive ETGs belonging to the LEG spectroscopic class. With respect to the first group, they follow more closely the L_{core} vs $L_{[O\ III]}$ relation.

Fig. 7 shows that the core dominance for this sub-sample ranges from $\log R$ ∼ -1 to ∼ 0 with a mean value of ∼-0.5. This distribution is significantly different from from that of 3CR/FRIs (with a >99.9% probability, according to a Kolmogorov Smirnoff test) while it is not distinguishable from the R distribution of CoreG. We remind that we estimated R as the ratio between the 7.5-GHz core emission and the total 1.4-GHz flux (NVSS), while for the 3CR/FRIs and CoreG we used the 5 GHz core flux against the total 1.4-GHz flux (NVSS). However, since the radio core emission has generally a flat spectrum this quantity is only weakly dependent on the frequency used for the core measurement and this comparison is robust.

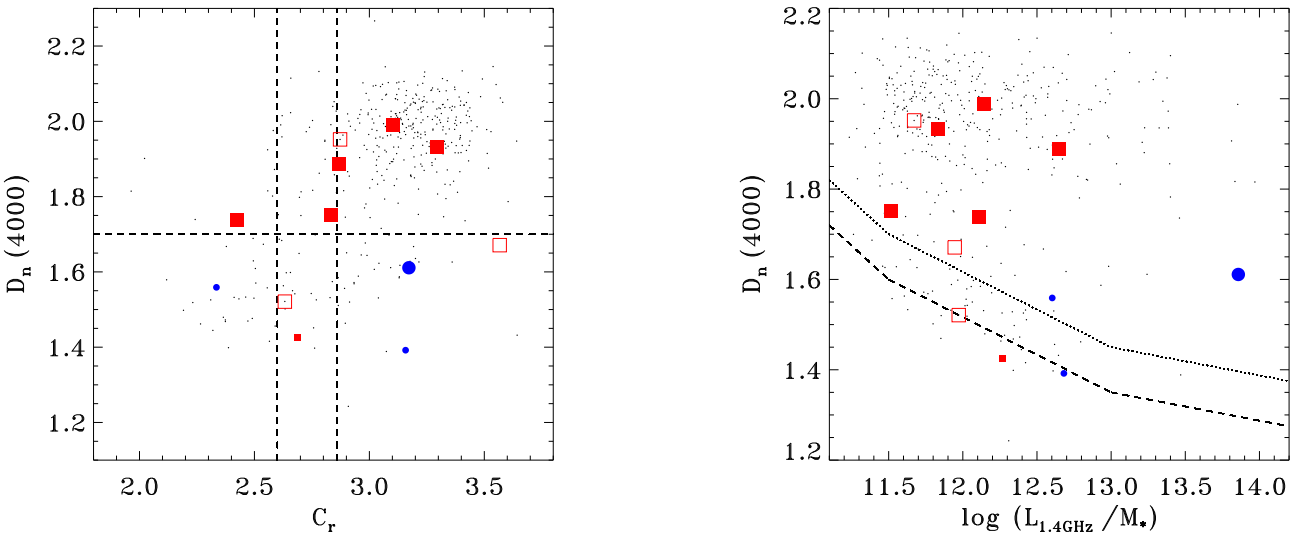

Fig. 6. Left panel: concentration index in the r band, C_r, versus the $D_n(4000)$ index. The vertical lines correspond to the two definition of ETGs (C_r > 2.86 or 2.60, see text for details), while the horizontal line separates the blue from red sources. Right panel: $D_n(4000)$ versus $L_{1.4\,\mathrm{GHz}}/M_*$. The dashed curve is the empirical separation between the star forming and AGN radio emitting sources, performed by Best et al. (2005) (read the text for details). The dotted curve is shifted 0.1 above in $D_n(4000)$ of the dashed curve, in order to separate the objects with a possible star-formation contribution to their radio emission. The small dot points correspond to the SDSS/NVSS sample studied by Baldi & Capetti (2010). The different color/shape symbols correspond to the different classes like in Fig. 1.

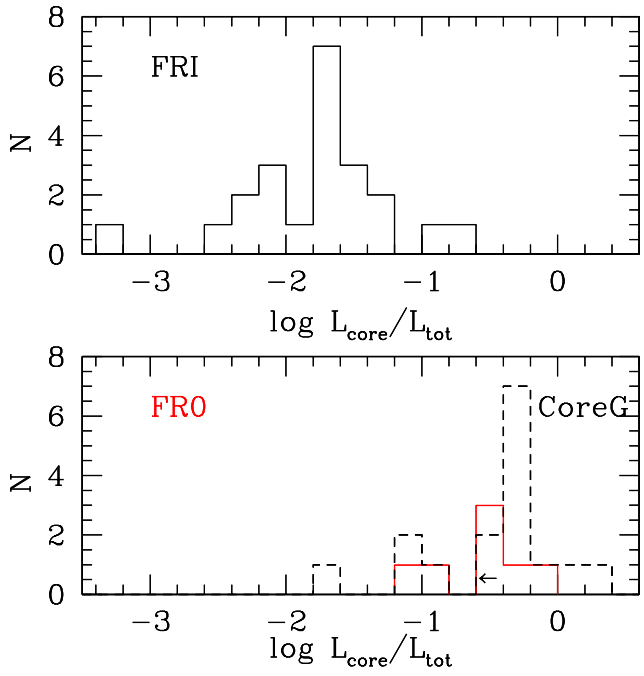

Fig. 7. Histograms of core dominance Log R = log (L_{core}/L_{tot}) for the 3CR/FR Is (black solid line), CoreG (black dashed line) and our sample of seven FR 0s (red solid line).

5. Discussion

The results discussed in the previous sections indicate that the twelve objects, belonging to the SDSS/NVSS sample and observed with the JVLA, can be divided in two main groups, corresponding to specific radio, spectroscopic, and photometric properties. Before discussing these groups in more detail, we treat here the only object that shows rather different properties. Not surprisingly, by exploring a sample of radio-sources, we found a classical extended RG, namely ID 625. As already mentioned it has a hybrid FR I/FRII morphology extending over ∼40 kpc. All its characteristics are typical of FR II sources considering its BH mass, the blue host color, its spectroscopic class (HEG), and its location in both the L_{core} and L_{tot} vs $L_{[O\,III]}$ diagram in the region populated by the FR II part of 3C sample (Chiaberge et al. 2002; Buttiglione et al. 2010; Chiaberge & Marconi 2011).

The first main group consists of four sources which are characterized by their low BH masses, mostly ∼10^7 $M_\odot$ and their blue color. Their radio and spectrophotometric properties indicate they are RQ AGN (Tab 4). The presence of an active nucleus is witnessed by their optical line ratios and equivalent widths, characteristic of AGN. Nonetheless, three of them shows a substantial contamination from star formation to their radio emission. The fourth object (ID 568) shows a double radio morphology with a size of 0.8 kpc and a steep spectrum, often observed in Seyfert galaxies (Edelson 1987; Nagar et al. 2005). In addition, its radio and line power locate this source in the area typical of the Seyfert galaxies. The contamination from RQ AGN (∼33% of the sample) is higher than observed in the whole SDSS/NVSS sample (Baldi & Capetti 2010). This is due to the fact that the selection criterion of this pilot sample based on the high [O III] equivalent width favors the inclusion of bright emission-line galaxies, which are preferentially RQ AGN.

The second group consists of seven sources, representing (together with the powerful source ID 625 discussed above)

the genuine RL AGN population in the SDSS/NVSS sample. They live in red massive ($\sim 10^{11}$ $M_\odot$) ETGs, have BH masses $\gtrsim 10^8$ $M_\odot$ and are spectroscopically classified as LEGs (apart from the HEG-spectrum FR I/FR II 625). All these properties are shared with FR I RGs (e.g., Zirbel 1996; Cao & Rawlings 2004; Floyd et al. 2008; Chiaberge et al. 1999; Baldi & Capetti 2008, 2009; Buttiglione et al. 2010). Furthermore, their radio core and [O III] luminosities lie in the range typical of FR Is. Therefore, all the nuclear and host characteristics of this group are indistinguishable from those of FR Is. Nonetheless, the JVLA observations presented here show compact radio structures (with a limit to their size of ~ 0.5 kpc or, in a few cases, extending by at most 1-3 kpc) and lead to an estimate of their (average) core dominance a factor of ∼30 higher than FR Is. The only feature distinguishing them from FR Is is then the substantial lack of extended radio emission. For such a paucity we define them *FR 0*.

5.1. The FR 0 population

The FR 0 classification corresponds to a combination of radio and spectro-photometric properties. In the radio band, FR 0s are characterized by a core responsible for a fraction larger than $\gtrsim$10% of the total emission with structures extending for, at most, a few kpc. In classical FR Is and FR IIs RGs the core dominance is typically $\lesssim$1% and their sizes are of tens or hundreds of kpc. (e.g, Morganti et al. 1993, 1997). The high FR 0 core dominance appears to be due to the paucity of extended radio emission, rather than to an enhanced radio core, since FR 0s and FR I show similar ratios of radio-core to emission line luminosity. In addition, the FR 0 definition involves the photometric/spectroscopic nuclear and host properties (e.g., BH mass, color, and emission line ratios, similar to FR Is), which distinguish them from the radio-sources associated with RQ AGN and star forming galaxies.

This new class of RGs is similar to the low-luminosity radio sources hosted in ETGs, studied by Slee et al. (1994), which contain parsec-scale radio cores and do not produce extended radio emission. Furthermore, recently, Sadler et al. (2014) found that the bulk of the 20-GHz RG population consists of compact radio sources lacking of extended radio emission, analogous to our FR 0s.

The CoreG fulfill the requirements for a FR 0 classification: they show kpc scale radio structures and are of high core dominance, they are hosted in red giant ellipticals and are characterized by LEG line ratios. They are ∼100 times less luminous than the FR 0s of the SDSS/NVSS sample discussed here. They smoothly extend the various nuclear multi-wavelengths relations seen in FR Is. In this sense they represent the low luminosity end of the FR 0 population that therefore extends at least down to a radio power of $\sim 10^{36}$ erg s^{-1}.

The small size and the steep spectra of FR 0s might suggest the presence of Compact Steep Sources (CSS), i.e. of rapidly growing young radio-sources (e.g. O'Dea 1998; Snellen et al. 2000). CSS show a correlation between the turnover frequency in their spectra and their linear sizes (e.g., Fanti et al. 1990; O'Dea 1998). The sizes of our FR 0 sources (<3 kpc) does not contrast with their steep spectra since the turnover might occur at lower frequencies than the lowest value sampled by our observations, 1.4 GHz. However, the core dominance of CSS, although generally more difficult to measure and uncertain with respect to more extended radio-sources, is much lower than in FR 0s (typically $\log R$ ∼-1 for quasars and $\log R$ ∼-2.4 for galaxies Saikia et al. 1995, 2001) ruling out a general association of the FR 0s with the CSS.

As reported in the Introduction, the vast majority of the SDSS/NVSS objects fulfill the FR 0 definition with the notable exception of the lack of a direct measurement of the core dominance, impossible from the FIRST images. Indeed, this was the main motivation to obtain the higher resolution data presented in the previous sections. Nonetheless, the possibility that they are generally high core dominance objects, and thence bonafide FR 0, appears to be reasonably founded. In fact, most of them (∼80 %) are unresolved or barely resolved in the FIRST maps, limiting their sizes to, at most, a few kpc. This is an indication that, similarly to the 7 objects studied, they have a deficit of extended radio emission with respect to classical extended RGs. It is clearly highly desirable to obtain proper radio data for a larger sample to base this conclusion on firmer ground. Therefore, if this result was confirmed for a larger sub-sample of the SDSS/NSS RGs, the FR 0 population would turn out to be the dominant class of RGs in the local Universe with a space density >100 times higher than 3C sources, as also suggested by Sadler et al. (2014).

FR 0s apparently differ from FR Is just for the lack of large scale radio structures. In the following we present two scenarios that can account for this specific property.

In the first scenario, the central engines of FR 0s and FR Is are indistinguishable and the paucity (and small size) of the extended radio emission is ascribed to an evolutionary effect. FR 0s might be young RGs that did not yet developed an extended radio structure. However, their number density should be smaller than that of FR Is, the opposite of what is observed. This scenario can hold if FR 0s are intermittent sources. Rapid AGN intermittency (see, e.g., Readhead et al. 1994; Reynolds 1997; Czerny et al. 2009) would prevent FR 0s from becoming well developed RGs. However, this does not explain why intermittency should affect only FR 0s, particularly considering the indications that accretion in FR Is and CoreG is associated with a long-lasting inflow of hot coronal gas (Allen et al. 2006; Balmaverde et al. 2008), related only to the host properties. Therefore, no differences would be expected between FR 0s and FR Is.

As a second scenario, the differences between FR 0s and FR Is might be due to a lower jet bulk speed Γ in FR 0s than in FR Is. In this scheme, the innermost regions of FR 0 and FR Is do not differ significantly since they share a common range of accretion rates (proved by the similarity in line emission luminosity and optical line ratios) and of radio core powers (which represent the synchrotron emission from the base of the jet). The different radio behavior should arise on a larger scale. In the hypothesis that jets in FR 0s are slower than FR Is, they are more subject to instabilities and entrainment (Bodo et al. 2013) and this causes their premature disruption. Indeed, the typical scale of the radio emission in FR 0s is smaller than the

core size of their hosts, a region characterized by a dense interstellar medium that obstructs the passage of the jet. This idea is supported, albeit with a small number statistics, by the absence of one-sided kpc scale morphologies among the FR 0s observed, the typical sign of relativistic jet boosting. The ultimate origin of the lower Γ factor in FR 0 is apparently not related to any directly observable quantity. We speculate that this could be due to a different spin of their central BH, by assuming a dependence between the BH spin and Γ, as suggested by, e.g., McKinney (2005), Tchekhovskoy et al. (2010), Chai et al. (2012), and Maraschi et al. (2012). The FR I radio morphology is produced only when the BH spin is close to its maximum value, while smaller spin values could be associated with FR 0s. Recently, Ghisellini et al. (2014) predicted a population of jetted sources which have smaller BH spin than classical RL AGN: the FR 0s might represent or be part of this population.

6. Summary and Conclusions

We present the observations of 12 objects with the JVLA in A-array configuration. These sources are selected from a large sample (cross-matching NVSS/FIRST and SDSS) which represents the bulk of the local radio-emitting AGN population (Baldi & Capetti 2010). Based on the FIRST radio maps, most of the sources are compact on an angular scale of 5″.

The new high-resolution observations at 1.4, 4.5, and 7.5 GHz reveal that they still show a compact morphology, extending at most over 1-3 kpc (with just one exception, a hybrid FR I/FR II which extends over ∼40 kpc). We isolate and measure the radio core component thanks to the new high-resolution maps or to the radio spectra. Furthermore, the SDSS survey provides with the spectro-photometric properties of the sample, such as, BH mass, host type, emission lines. Based on these properties, we divide the sample into two groups.

The first group consists of four sources which represent the RQ AGN contamination to the SDSS/NVSS sample. They have small BH masses (mostly $\sim 10^7$ $M_\odot$) associated with blue galaxies which show evidences of star formation.

The second group consists of seven RL AGN in red massive (M_* $\sim 10^{11}$ $M_\odot$ and BH masses $\gtrsim 10^8$ $M_\odot$) ETGs spectroscopically classified as LEG. All these characteristics are shared by local FR Is. In particular, the members of this group have similar radio and [O III] line luminosities of FR Is, lying on the same relation; however, they show a core dominance higher than in FR Is by a factor ∼30. What distinguishes this group from FR Is is one single aspect: the lack of substantial extended emission. For this characteristic we define these objects 'FR 0'. This new RG class is consistent with a sub-class of Gigahertz-Peaked Spectrum (GPS) radio sources, proposed by Tingay & Edwards (2015), with low luminosity and with jet-dominated compact morphologies similar to FR Is and lacking of extended radio emission. Furthermore, recently, Sadler et al. (2014), studying the 20-GHz radio-source population in the local Universe, suggest that the FR 0s might be a mixed population of young CSS and GPS radio galaxies.

What causes the deficit of extended radio emission in FR 0s? We discuss two possible interpretations. The first scenario proposes that the FR 0s consist in young intermittent radio sources that will eventually evolve into extended RGs. However, this contrasts with the picture in which low luminosity RGs are powered by continuous accretion of hot gas from their X-ray coronae. Furthermore, it does not explain why the intermittency should only occur in FR 0s and not in FR Is, considering the similarity of their nuclear and host properties.

The second scenario suggests that FR 0s have smaller jet Lorentz factors Γ than FR Is: their jets are less stable against entrainment and their passage through the dense ISM region of the central regions of their hosts causes their premature disruption. This low-Γ scenario can be tested by looking at the asymmetry between the opposite jets in FR 0s, a parameter directly linked to the jet speed. Although twin symmetric jets are common in FR Is, they often have one jet substantially brighter than the other on kpc scale (e.g., Parma et al. 1987). This indicates that the high Doppler factors derived for FR Is on pc scale (based on the detection of superluminal motions, e.g., Giovannini et al. 2001, and, indirectly, on the association with BL Lac objects in the AGN unified model, e.g. Urry & Padovani 1995) are preserved to larger scales. In the present sample we find that all three FR 0s with an extended radio structure are two-sided and rather symmetric. The number is too small to draw any firm conclusion (and two-sided jets are expected to be more common than a one-sided morphology in a randomly oriented sample) but it is consistent with this hypothesis. We speculate that the ultimate difference between FR 0s and FR Is is the spin of their BH, being smaller for FR 0s.

High resolution imaging of a larger sample of local low luminosity radio sources is needed to put this result on firmer statistical ground and confirm the presence of the FR 0 population. In order to improve the efficiency of such a survey, the results obtained in this study indicate that it should be focused on objects with a LEG spectrum, hosted in red early type galaxies. If the FR 0 population was confirmed, they would represent the bulk of the RL AGN in the local Universe with a large impact on our view of the low-luminosity radio-emitting population.

Appendix A: Notes on the extended radio-sources

We report here notes on the structure of the extended radio-sources in the sample.

ID 547: while at 1.4 and 4.5 GHz it is only marginally resolved, a clear twin-jet morphology is revealed at the higher frequency (Fig. A.1). The two jets are rather straight and symmetric, extending for for about 1″ on each side of the nucleus along PA ∼ -40°.

ID 568: its radio morphology is double (∼0.″5 in size) with PA = ∼130° (Fig. A.2). The position of the two lobes are (00^h 34′ 43.″51 -00^d 02′ 27.″06) and (00^h 34′ 43.″48 -00^d 02′ 26.″67) whose fluxes at 4.5 and 7.5 are respectively: 15.3 and 6.7 mJy for the former component and 8.4 and 5.3 mJy for the latter. The resolution is insufficient to resolve sub-structures or the presence of a radio core.

ID 590: the source is point-like in L band, while at high frequencies the source is elongated with PA=45° with a size of 0.″8 (Fig. A.3) with a morphology suggestive of a bent two-sided jet structure.

ID 625: this source shows at low resolution a central emission and a double structure in the NS direction (Fig. A.4) on a scale of 36″, ∼40 kpc. Toward the South only a diffuse lobe is visible, while toward the North there is a bright jet-like structure, typical of FR Is, terminating into a diffuse plume. This radio structure is typical of the so-called hybrid radio-sources (Gopal-Krishna & Wiita 2000). At high resolution the nuclear source is resolved and rather complex. A compact flat spectrum region (located at $01^h\ 48'\ 16\overset{s}{.}25\ 00^d\ 19'\ 44\overset{''}{.}9$) is identified as the radio core based on its flat spectral index (0.05 between 4.5 and 7.5 GHz). From the core a one-sided emission is visible, pointing at SW, but it sharply bends toward the NE after ∼ 2″ from the core and it then enters the N lobe. Two knots are visible in the 7.5 GHz image with spectral index 0.6 and 1.16 respectively. The large jet bending and the jet asymmetry suggest that in this source is present a relativistic jet at a small angle with respect to the line of sight.

Acknowledgements. RDB was supported at the Technion by a fellowship from the the Lady Davis Foundation. We thank the anonymous referee for the constructive comments that have helped us to improve the paper.

References

Allen, S. W., Dunn, R. J. H., Fabian, A. C., Taylor, G. B., & Reynolds, C. S. 2006, MNRAS, 372, 21
Baldi, R. D. & Capetti, A. 2008, A&A, 489, 989
Baldi, R. D. & Capetti, A. 2009, A&A, 508, 603
Baldi, R. D. & Capetti, A. 2010, A&A, 519, A48+
Baldi, R. D., Chiaberge, M., Capetti, A., et al. 2010, ApJ, 725, 2426
Baldwin, J. A., Phillips, M. M., & Terlevich, R. 1981, PASP, 93, 5
Balmaverde, B., Baldi, R. D., & Capetti, A. 2008, A&A, 486, 119
Balmaverde, B. & Capetti, A. 2006, A&A, 447, 97
Balmaverde, B., Capetti, A., & Grandi, P. 2006, A&A, 451, 35
Balogh, M. L., Morris, S. L., Yee, H. K. C., Carlberg, R. G., & Ellingson, E. 1999, ApJ, 527, 54
Bell, E. F., McIntosh, D. H., Katz, N., & Weinberg, M. D. 2003, ApJS, 149, 289
Bell, E. F., Zheng, X. Z., Papovich, C., et al. 2007, ApJ, 663, 834
Bernardi, M., Shankar, F., Hyde, J. B., et al. 2010, MNRAS, 404, 2087
Best, P. N. & Heckman, T. M. 2012, MNRAS, 421, 1569
Best, P. N., Kauffmann, G., Heckman, T. M., & Ivezić, Ž. 2005, MNRAS, 362, 9
Bodo, G., Mamatsashvili, G., Rossi, P., & Mignone, A. 2013, MNRAS, 434, 3030
Buttiglione, S., Capetti, A., Celotti, A., et al. 2010, A&A, 509, A6+
Cao, X. & Rawlings, S. 2004, MNRAS, 349, 1419
Capetti, A. & Baldi, R. D. 2011, A&A, 529, A126
Chai, B., Cao, X., & Gu, M. 2012, ApJ, 759, 114
Chiaberge, M., Capetti, A., & Celotti, A. 1999, A&A, 349, 77
Chiaberge, M., Capetti, A., & Celotti, A. 2002, A&A, 394, 791
Chiaberge, M. & Marconi, A. 2011, MNRAS, 416, 917
Czerny, B., Siemiginowska, A., Janiuk, A., Nikiel-Wroczyński, B., & Stawarz, Ł. 2009, ApJ, 698, 840
Edelson, R. A. 1987, ApJ, 313, 651
Fanti, R., Fanti, C., Schilizzi, R. T., et al. 1990, A&A, 231, 333
Floyd, D. J. E., Axon, D., Baum, S., et al. 2008, ApJS, 177, 148
Ghisellini, G., Tavecchio, F., Maraschi, L., Celotti, A., & Sbarrato, T. 2014, Nature, 515, 376
Giovannini, G., Cotton, W. D., Feretti, L., Lara, L., & Venturi, T. 2001, ApJ, 552, 508
Gopal-Krishna & Wiita, P. J. 2000, A&A, 363, 507
Heckman, T. M. 1980, A&A, 87, 152
Kauffmann, G., Heckman, T. M., White, S. D. M., et al. 2003, MNRAS, 341, 33
Kewley, L. J., Groves, B., Kauffmann, G., & Heckman, T. 2006, MNRAS, 372, 961
Maraschi, L., Colpi, M., Ghisellini, G., Perego, A., & Tavecchio, F. 2012, Journal of Physics Conference Series, 355, 012016
McKinney, J. C. 2005, ApJ, 630, L5
Morganti, R., Killeen, N. E. B., & Tadhunter, C. N. 1993, MNRAS, 263, 1023
Morganti, R., Oosterloo, T. A., Reynolds, J. E., Tadhunter, C. N., & Migenes, V. 1997, MNRAS, 284, 541
Nagar, N. M., Falcke, H., & Wilson, A. S. 2005, A&A, 435, 521
Nakamura, O., Fukugita, M., Yasuda, N., et al. 2003, AJ, 125, 1682
O'Dea, C. P. 1998, PASP, 110, 493
Parma, P., Fanti, C., Fanti, R., Morganti, R., & de Ruiter, H. R. 1987, A&A, 181, 244
Readhead, A. C. S., Xu, W., Pearson, T. J., Wilkinson, P. N., & Polatidis, A. G. 1994, in Compact Extragalactic Radio Sources, ed. J. A. Zensus & K. I. Kellermann, 17–+
Reynolds, C. S. 1997, MNRAS, 286, 513
Sadler, E. M., Ekers, R. D., Mahony, E. K., Mauch, T., & Murphy, T. 2014, MNRAS, 438, 796
Saikia, D. J., Jeyakumar, S., Salter, C. J., et al. 2001, MNRAS, 321, 37
Saikia, D. J., Jeyakumar, S., Wiita, P. J., Sanghera, H. S., & Spencer, R. E. 1995, MNRAS, 276, 1215
Shen, S., Mo, H. J., White, S. D. M., et al. 2003, MNRAS, 343, 978
Slee, O. B., Sadler, E. M., Reynolds, J. E., & Ekers, R. D. 1994, MNRAS, 269, 928
Snellen, I. A. G., Schilizzi, R. T., Miley, G. K., et al. 2000, MNRAS, 319, 445
Strateva, I., Ivezić, Ž., Knapp, G. R., et al. 2001, AJ, 122, 1861
Tchekhovskoy, A., Narayan, R., & McKinney, J. C. 2010, ApJ, 711, 50
Tingay, S. J. & Edwards, P. G. 2015, ArXiv e-prints
Tremaine, S., Gebhardt, K., Bender, R., et al. 2002, ApJ, 574, 740
Urry, C. M. & Padovani, P. 1995, PASP, 107, 803
Zirbel, E. L. 1996, ApJ, 473, 713

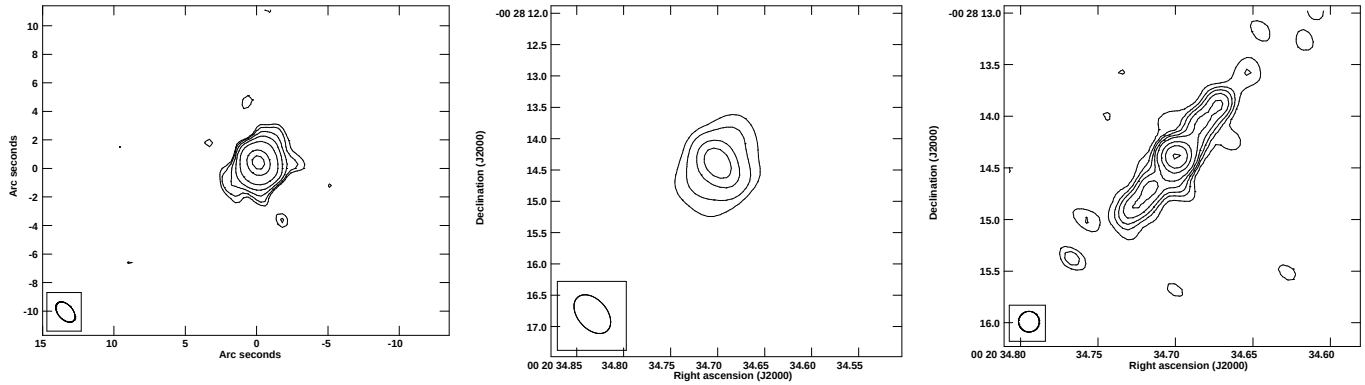

Fig. A.1. JVLA images of ID 547 at 1.4, 4.5 and 7.5 GHz. The HPBWs and noise levels are reported in Tab. 2. Levels are respectively: 0.15 0.2 0.3 0.5 1 3 5 mJy/beam; 0.3 0.5 0.9 1.3 mJy/beam; 0.03 0.05 0.07 0.1 0.15 0.3 0.5 0.9 mJy/beam

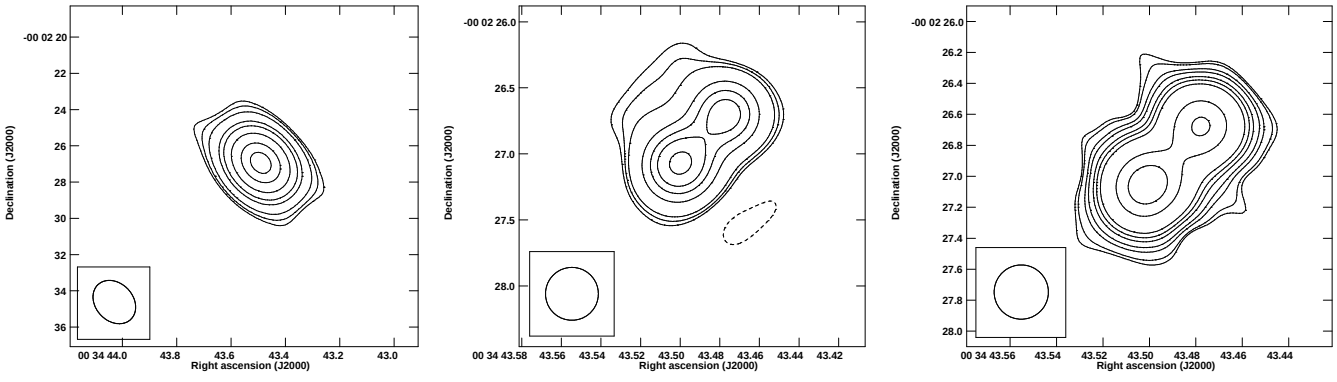

Fig. A.2. JVLA images of ID 568 at 1.4, 4.5 and 7.5 GHz. The HPBWs and noise levels are reported in Tab. 2. Levels are respectively: 0.3 0.5 1 3 5 10 20 30 mJy/beam; -0.5 0.5 0.7 1 3 5 7 10 20 30 50 70 mJy/beam; 0.07 0.1 0.2 0.3 0.5 0.7 1 3 5 mJy/beam

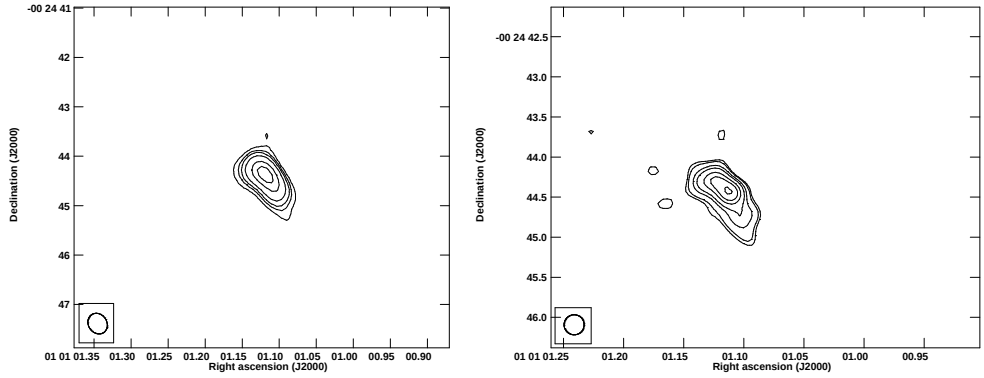

Fig. A.3. JVLA images of ID 590 at 4.5 and 7.5 GHz. The HPBWs and noise levels are reported in Tab. 2. Levels are respectively: 0.1 0.2 0.3 0.5 1 1.5 mJy/beam; 0.07 0.1 0.2 0.3 0.5 0.7 1 mJy/beam

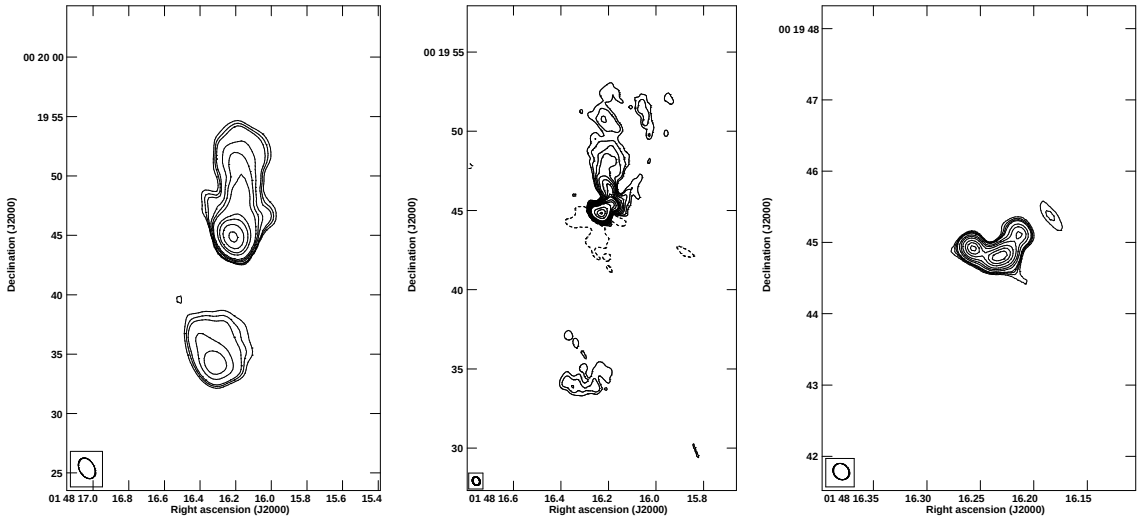

Fig. A.4. JVLA images of ID 625 at 1.4, 4.5 and 7.5 GHz. The HPBWs and noise levels are reported in Tab. 2. Levels are respectively: 2 2.5 3 5 7 10 30 50 100 200 mJy/beam; -0.2 0.2 0.3 0.5 0.7 1 1.5 2 2.5 3 5 7 10 30 50 70 mJy/beam; 1.5 2 2.5 3 5 7 10 15 20 25 mJy/beam